



University of Technology, Sydney

Faculty of Engineering

**Fault Location and Forewarning
On Transmission Systems Using
Travelling Wave Transients**

Darren John Spoor

**Thesis submitted in fulfilment of the requirement for the
Degree of Doctor of Philosophy in Engineering**

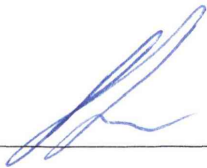
September 2006

Statement of Authorship & Originality

I certify that this thesis has not previously been submitted for a degree nor has it been submitted as part of requirements for a degree except as fully acknowledged within the text.

I also certify that the thesis has been entirely written by me. Any help that I have received in my research work and the preparation of the thesis itself has been acknowledged. In addition, I certify that all information sources and literature used are indicated in the thesis.

Signature of Candidate



Acknowledgments

There are several people who have provided valuable guidance and support while I have researched this topic over the last few years.

Specifically, two people were instrumental in encouraging me to search for understanding in a formal research environment. Prof. Jianguo Zhu, the principal supervisor, from the University of Technology Sydney has always been supportive and ready to provide assistance at any time. All this for a student who took time to get married in 2004, changed positions within TransGrid several times, and recently changed employers. Given this extended commitment, he has regularly found time to guide and answer my questions.

This assistance was matched by Colin Parker who prompted me to fully engage this topic whilst working for TransGrid. Similarly, Don Geddey instilled a keen interest in computer based simulation and transient analysis and was always there to review and critique results.

Kevin Hinkley, Fred Rodrigues and Steve Jones all deserve recognition for guiding me towards travelling wave fault location and assist in its implementation on the TransGrid network. They also initially encouraged me to document my work in conference papers and in other formats.

I also must acknowledge Andrew Kingsmill for his friendship and assistance in organising high voltage tests and measurement of data from the high voltage network. Similarly, appreciation must go to Phillip Nichols, a student from the University of Sydney who spent a brief time at TransGrid on work experience. His assistance in the later stages of this research was very helpful.

Nevertheless, the final thanks must go to my wife, Rebecca Spoor, for coping with the many hours of work each night as this thesis progressed. She has also carefully spent much time reading this document.

This whole experience, whilst physically draining at times, has been an incredibly valuable experience. However, it could not have been completed without the efforts and assistance of all those acknowledged above.

Abstract

This thesis examines the main circuit modelling fundamentals and fault location techniques that may be applied to electricity transmission networks. Using a statistical comparison, it then investigates both impedance and travelling wave based fault location methods. This appears to be a novel comparison as no publications have been identified which draw conclusions on the accuracy of these fault location techniques. This work subsequently led TransGrid to install a new commercial travelling wave fault location system on the New South Wales 330kV transmission network.

Following the commissioning of this system, there was an ongoing process to store data that was being observed by the travelling wave recorders. This data was later cross-referenced to determine the fault location, and the waveform interpreted to identify the source of the travelling wave transient. However, this analysis has revealed that the theoretical accuracy of this travelling wave system was not as good as previously expected from publication.

The source of the degradation was tracked down and found to centre on the frequency response of the coupling transducers used by most conventional travelling wave recording hardware. These errors are not currently considered in publication but can result in several kilometres of uncertainty in a fault location calculation. Hence, it can be concluded that the use of conventional substation current transducers can introduce additional uncertainty into travelling wave fault location calculations.

The source and nature of this uncertainty has subsequently led to the development of a novel unsynchronised fault location algorithm based on the continuous wavelet transform. This new technique also uses an assessment of waveform polarity to distinguish between signals generated by solid or incipient line faults.

Several unusual events have also been observed which have led to a number of new developments in fault location and forewarning. These include specific requirements for impedance algorithms during unearthed inter-circuit faults on double circuit lines.

Similarly, this thesis presents the development of a new method to forewarn of faults within oil impregnated current transformers. This has been based on the high frequency transients observed by the travelling wave system prior to the failure of a 330kV current transformer.

This thesis also identifies significant potential for travelling wave techniques to forewarn of developing insulator faults on overhead circuits.

Table of Contents

<i>Statement of Authorship & Originality</i>	<i>i</i>
<i>Acknowledgments</i>	<i>ii</i>
<i>Abstract</i>	<i>iii</i>
<i>Table of Contents</i>	<i>v</i>
<i>List of Illustrations</i>	<i>ix</i>
<i>List of Tables</i>	<i>xv</i>
<i>Nomenclature</i>	<i>xvi</i>
1. Introduction	1
2. Literature Review	7
2.1 Introduction	8
2.2 Fault Location on Transmission Circuits	9
2.3 Circuit Modelling Fundamentals	11
2.3.1 Fault Analysis and Sequence Techniques	11
2.3.2 Steady State Transmission Circuit Models	12
2.3.3 Travelling Waves and the Modal Domain	21
2.4 Transient Simulation Software	31
2.4.1 Calculation Methodology	31
2.4.2 Lumped Transmission Line Models	34
2.4.3 Distributed Transmission Line Models	35
2.4.4 Example Modal Calculations for Hypothetical Transmission Circuits	40
2.5 Impedance Based Fault Location	46
2.5.1 Single Ended Fault Location	47
2.5.2 Double Ended Fault Location	52
2.5.3 Impact of Fault and Power System Parameters	56
2.6 Travelling Wave Fault Location	64
2.6.1 Classical Travelling Wave Algorithms	65
2.6.2 Documented Accuracy of Travelling Wave Implementations	71
2.6.3 Signal Processing for Travelling Wave Methods	73
2.7 Conclusion	85
3. Comparative Analysis of Fault Location Algorithms	86
3.1 Introduction	87
3.2 Transmission Line and Fault Modelling	87
3.3 Sensitivity Analysis	90
3.3.1 Impedance Based Algorithms	90
3.3.2 Parameter Sensitivity in the Travelling Wave Algorithm	91

3.4	Probabilistic Fault Location Analysis	94
3.4.1	Fault Statistics	95
3.4.2	Line Loading	95
3.4.3	Fault Resistance	96
3.4.4	Source Impedance	97
3.5	Results and Discussion	97
3.5.1	The Distance Algorithm Based on Impedance Calculations	97
3.5.2	The Distance Algorithm Based on Reactance Calculations	98
3.5.3	The Takagi Algorithm	99
3.5.4	The Takagi Algorithm with Mutual Coupling Compensation	101
3.5.5	The Synchronised Phasor Algorithm	101
3.5.6	The Unsynchronised Phasor Algorithm	102
3.5.7	The Unsynchronised Phasor Algorithm with Long Line Compensation	103
3.5.8	The Type D Travelling Wave Algorithm	105
3.6	Selection of Fault Location Technique	106
3.7	The Travelling Wave Fault Location System	107
3.8	Comparison with Experimental Data	110
3.9	Conclusion	111
4.	<i>Fault Location and Protection for Inter-Circuit Faults</i>	113
4.1	Introduction	114
4.1.1	Background	114
4.2	Inter-Circuit Faults	118
4.2.1	Impedance-Based Distance Algorithm	119
4.2.2	Distance Algorithm based on Observed Reactance	119
4.2.3	The Takagi Algorithm	120
4.2.4	Takagi Algorithm with Mutual Coupling Compensation	120
4.2.5	Synchronised Phasors	121
4.2.6	Unsynchronised Phasors	121
4.2.7	Travelling Wave Fault Location	122
4.3	Distance Protection and Inter-circuit Faults	123
4.3.1	Fault Detection	125
4.3.2	Relay Impedance Characteristics	126
4.3.3	Protective Zones of Operation	126
4.4	Distance Protection Schemes	127
4.4.1	Permissive Under-reach	128
4.4.2	Permissive Over-reach	129
4.4.3	Blocking Schemes	130
4.4.4	Current Differential	131
4.5	Case Study Based on the Queensland to New South Wales Interconnector	131
4.5.1	Selection of Zone Settings	132
4.5.2	Impedance Variations for Inter-Circuit Faults	134
4.5.3	Source Impedance Considerations	138
4.5.4	Line to Source Impedance Ratio	141
4.5.5	Line Protection Implications	142

4.5.6	Uncoupled Line Topologies	144
4.6	Conclusion	145
5.	<i>Observed Uncertainty with Travelling Wave Calculations</i>	147
5.1	Introduction	148
5.2	Transient Propagation Time	148
5.2.1	Observed Distribution in the Signal Propagation Time	153
5.2.2	A Simple Comparison of Signal Processing Techniques	155
5.3	Uncertainty in Synchronised Timing	158
5.4	Filtering Imposed by Substation Transducers	159
5.4.1	Transfer Function Estimation	162
5.4.2	Experimental Methods to Measure Transducer Filtering	167
5.5	Conclusion	183
6.	<i>Simulating the Performance of Substation Transducers</i>	185
6.1	Introduction	186
6.2	Substation Current Transformers	186
6.3	Development of a Current Transformer Model	190
6.3.1	The Resistance of the Toroidal Core	194
6.3.2	The Leakage Inductance of the Toroidal Core	196
6.3.3	The Magnetising Characteristic of the Toroidal Core	197
6.3.4	The CT Bushing Capacitances	199
6.3.5	The CT Stray Capacitance	200
6.3.6	The Transformer Model	202
6.4	Substation Secondary Cabling	202
6.5	The Current Transformer Burden	208
6.6	The Interposing CT and the Travelling Wave Recorder	209
6.7	Equivalent Electrical Model	217
6.8	Conclusion	219
7.	<i>Unsynchronised Travelling Wave Fault Location</i>	220
7.1	Introduction	221
7.2	Transducer Selection and Frequency Response	222
7.3	The Unsynchronised Travelling Wave Fault Location Algorithm	224
7.3.1	Discrete and Continuous Wavelet Applications	224
7.3.2	Simulated Solid and Incipient Faults	227
7.3.3	Observed Solid and Incipient Faults on the TransGrid Network	233
7.3.4	The proposed algorithm	235
7.3.5	High Impedance Faults	236
7.3.6	Accuracy of the Single Ended Algorithm	237
7.4	Conclusion	240

8. Forewarning Of Catastrophic Insulation Faults	241
8.1 Introduction	242
8.1.1 The Failure of a 330kV Current Transformer	243
8.1.2 Condition Monitoring Systems	248
8.2 On-Line Techniques Used At Bayswater	250
8.2.1 Radio Based Systems	250
8.2.2 DDF and Insulation Resistance	252
8.3 Observed High Frequency Transients	255
8.3.1 Observed Travelling Wave Signals	256
8.4 Partial Discharge Detection	258
8.4.1 Partial Discharges	260
8.5 Proposed Monitoring Technique	264
8.5.1 Background Electrical Noise	265
8.6 The On-Line Monitor	269
8.7 Testing of the CT Monitor	272
8.7.1 Testing With a Simulated Partial Discharge	273
8.7.2 High Voltage Testing	277
8.8 Conclusion	289
9. Conclusions and Future Work	291
9.1 Conclusions	292
9.2 Future Work	293
10. Appendices	297
A.1 List of publications based on thesis work	298
A.2 Parameter sensitivity of fault location algorithms	300
A.3 Substation source impedance data	305
A.4 TransGrid 330kV network (2006)	306
A.5 Transfer function estimation	307
A.6 ATP input data cards	308
References	353

List of Illustrations

Figure 2-1. Simple model of a multiphase transmission circuit	13
Figure 2-2. Location of the propagation modes in transmission circuits	24
Figure 2-3. Independent modes of propagation within cable circuits	24
Figure 2-4. Transient network analyser [17]	31
Figure 2-5. Example nodal network [17]	32
Figure 2-6. Simulated phase currents during an earth fault 0km from the observer	36
Figure 2-7. Simulated phase currents during an earth fault 100km from the observer	36
Figure 2-8. Variation of zero and positive sequence resistance with frequency [7, 17]	38
Figure 2-9. Variation of zero and positive sequence inductance with frequency [7, 17]	38
Figure 2-10. J. Marti's weighting function [17].	39
Figure 2-11. Cross-bonding configuration applied along hypothetical cable route	40
Figure 2-12. Hypothetical 330kV conductor arrangement	44
Figure 2-13. Simple fault location representation based on a double ended topology	53
Figure 2-14. Phasing techniques	60
Figure 2-15. Single and dual circuit configurations	61
Figure 2-16. Single ended Takagi algorithm	63
Figure 2-17. Double ended synchronised phasors algorithm	64
Figure 2-18. Travelling wave fault location - method A	66
Figure 2-19. Travelling wave fault location - method B	67
Figure 2-20. Travelling wave fault location - method C	68
Figure 2-21. Travelling wave fault location - method D	69
Figure 2-22. Travelling wave fault location - method E	70
Figure 2-23. Frequency versus time characteristic of the Fourier transform [54]	75
Figure 2-24. Frequency versus time characteristic of the windowed Fourier transform [54]	75
Figure 2-25. The scale, shift and correlate process involved with the continuous wavelet transform applied to an observed circuit breaker transient	80
Figure 2-26. Continuous wavelet transform coefficients obtained from applying the 'symlets2' wavelet to an observed circuit breaker transient	80
Figure 2-27. 'Frequency versus time' characteristic of the Wavelet Transform	81
Figure 2-28. One stage of the DWT filtering process using a circuit breaker transient and a 'symlets2' wavelet	82
Figure 2-29. The 'Daubenchies2' wavelet and the corresponding pseudo-frequency [54]	83
Figure 2-30. Pseudo-frequencies of several common wavelets, at various scales	83
Figure 2-31. Examples of some wavelet function families	84
Figure 3-1. The electrical configuration of the Sydney West to Bayswater transmission line	88
Figure 3-2. Simple dual circuit model	89
Figure 3-3. Percentage increase in conductor length over span length at 20 °C	94
Figure 3-4. Load duration on the Sydney West to Bayswater 330kV circuit	96
Figure 3-5. Distribution of fault resistance	96
Figure 3-6. The impedance algorithm applied to a single circuit	98
Figure 3-7. The impedance algorithm applied to a double circuit line	98
Figure 3-8. The reactance algorithm applied to a single circuit	99
Figure 3-9. The reactance algorithm applied to a double circuit line	99
Figure 3-10. The Takagi algorithm applied to a single circuit	100
Figure 3-11. The Takagi algorithm applied to a double circuit line	100
Figure 3-12. The modified Takagi algorithm applied to a double circuit line	101
Figure 3-13. The synchronised phasor algorithm applied to a single circuit	102
Figure 3-14. The synchronised phasor algorithm applied to a double circuit line	102
Figure 3-15. The unsynchronised phasor algorithm applied to a single circuit	103
Figure 3-16. The unsynchronised phasor algorithm applied to a double circuit line	103
Figure 3-17. The unsynchronised algorithm with compensation for line capacitance when applied to a single circuit	104

Figure 3-18. The unsynchronised algorithm with compensation for line capacitance when applied to a double circuit line	104
Figure 3-19. Calibrated travelling wave algorithm	105
Figure 3-20. 2.5% error in the line length or modal velocity	106
Figure 3-21. The Hathaway (TWS) monitoring station	108
Figure 3-22. Installation of the Hathaway (TWS) monitoring station	109
Figure 3-23. The distributed travelling wave fault location system	109
Figure 4-1. Sydney South Substation and its 330kV feeders (Refer to Appendix 3)	115
Figure 4-2. The bushfire traversing the mountains (as seen from Sydney South substation) moments before the phase-to-phase inter-circuit fault occurred	117
Figure 4-3. Phase configuration for the inter-circuit fault simulation	118
Figure 4-4. Error distribution for the basic distance algorithm applied to an inter-circuit fault	119
Figure 4-5. Error distribution for the reactive distance algorithm when applied to an inter-circuit fault	119
Figure 4-6. Error distribution for the Takagi algorithm when applied to an inter-circuit fault	120
Figure 4-7. Error distribution for the modified Takagi algorithm when applied to an inter-circuit fault	120
Figure 4-8. Error distribution for the synchronised algorithm when applied to an inter-circuit fault	121
Figure 4-9. Error distribution for the unsynchronised algorithm, applied to an inter-circuit fault	122
Figure 4-10. The compensated unsynchronised algorithm when applied to an inter-circuit fault	122
Figure 4-11. The travelling wave algorithm when applied to an inter-circuit fault	123
Figure 4-12. Protection zone grading of mho distance elements	127
Figure 4-13. The permissive under-reach distance zones and the required communication acceleration between the protection relays	128
Figure 4-14. The permissive over-reach distance zones and the required communication acceleration between the protection relays	129
Figure 4-15. The blocking scheme distance zones and the required communication acceleration between the protection relays	130
Figure 4-16. Phase element impedance plot for an un-transposed line	134
Figure 4-17. Under-reaching effect associated with inter-circuit faults on transmission lines constructed with a high impedance phasing	135
Figure 4-18. Earth element impedance plot for an un-transposed line	136
Figure 4-19. Phase element impedance plot for a transposed line	136
Figure 4-20. Earth element impedance plot for a transposed line	137
Figure 4-21. Consideration of earth impedance loci	138
Figure 4-22. Impedances observed by phase elements for source impedance ratios of 1:1 and 2:1	138
Figure 4-23. Impedance loci observed from the weaker source terminal	139
Figure 4-24. Impedance loci observed from the stronger source terminal	139
Figure 4-25. Earth element impedance plot for a mho relay with a 100% forward reach	140
Figure 4-26. Maximum phase element under-reach observed for variations in the source impedance ratio.	140
Figure 4-27. Phase element impedance for a 1:1 SR with a variation in the line impedance	141
Figure 4-28. Earth element for a 1:1 SR with a variation in the line impedance	142
Figure 4-29. Sections of the line which are blind to inter-circuit faults, or suffer a loss of distance margin when protected with permissive under-reaching schemes	143
Figure 4-30. Sections of the line which suffer a loss of distance margin to inter-circuit faults when protected with permissive over-reaching schemes	144
Figure 4-31. Under-reach experienced by a hypothetically uncoupled circuit	145
Figure 4-32. Partially uncoupled dual circuit topology	145
Figure 5-1. High frequency circuit breaker transient observed at Sydney West	149
Figure 5-2. High frequency circuit breaker transient observed at Bayswater	149
Figure 5-3. High frequency earth fault transient observed at Sydney West	150
Figure 5-4. High frequency earth fault transient observed at Bayswater	150
Figure 5-5. Fault transient observed on each phase during a phase to earth fault (5 th January 2002)	151
Figure 5-6. Modal analysis of the phase to earth fault (5 th January 2002)	151

Figure 5-7. A circuit breaker operation observed at Munmorah on 23 line (13 th November 2001)	152
Figure 5-8. An A phase to earth fault observed at Sydney West on 32 line (14 th November 2001)	153
Figure 5-9. Calculated signal propagation travelling times from 38 circuit breaker operations	154
Figure 5-10. correlation between travel time and time of day	155
Figure 5-11. correlation between travel time and current prior to the event	155
Figure 5-12. A fault detected at Sydney West on the line to Bayswater (3rd December 2001)	157
Figure 5-13. Application of the continuous wavelet transform using a variety of wavelet functions	158
Figure 5-14. Average spectra of 38 CB signals seen respectively at Sydney West and Bayswater	160
Figure 5-15. Average spectra of 9 phase to phase signals seen at Sydney West and Bayswater	160
Figure 5-16. Average spectra of 4 earth fault signals observed at Sydney West and Bayswater	160
Figure 5-17. Average spectra of one lightning transient observed respectively at Sydney West and Bayswater	161
Figure 5-18. Travelling wave transients observed on the ScottishPower transmission system [21]	162
Figure 5-19. CB Transient at Sydney West with the matched transfer function response	164
Figure 5-20. A pole zero map of the circuit breaker transients observed at Sydney West	165
Figure 5-21. A pole zero map of the circuit breaker transients observed at Bayswater	165
Figure 5-22. Travelling wave fault location error distribution using pole locations from Table 5-2	166
Figure 5-23. Travelling wave trigger delay using the pole locations from Table 5-2	167
Figure 5-24. Protection secondary cabling used respectively at Bayswater and Sydney West	167
Figure 5-25. Installation of the travelling wave recorder in the switchyard	168
Figure 5-26. Time domain signal and spectra recorded at the base of the current transformer	169
Figure 5-27. Time domain signal and spectra recorded in the substation control room	170
Figure 5-28. A circuit breaker transient observed in the substation switchyard	170
Figure 5-29. A circuit breaker transient observed in the substation control room	170
Figure 5-30. Time domain signal and spectra recorded in the substation switchyard	172
Figure 5-31. Time domain signal and spectra recorded in the substation control room	172
Figure 5-32. Modal domain signal and FFT spectral coefficients observed in the switchyard	173
Figure 5-33. Modal domain signal and FFT coefficients observed in the substation control room	173
Figure 5-34. Transfer function estimation using the A-C aerial mode (0-300kHz)	174
Figure 5-35. Transfer function estimation using the A-B aerial mode (0-300kHz)	175
Figure 5-36. Transfer function estimation using the B-C aerial mode (0-300kHz)	175
Figure 5-37. Time domain signal and spectra recorded in the Sydney West switchyard	176
Figure 5-38. Time domain signal and spectra recorded in the substation control room	177
Figure 5-39. Modal domain signal and FFT coefficients observed in the switchyard	177
Figure 5-40. Modal domain signal and FFT coefficients observed in the substation control room	178
Figure 5-41. Transfer function estimation using the A-C aerial mode (0-300kHz)	179
Figure 5-42. Transfer function estimation using the A-B aerial mode (0-300kHz)	179
Figure 5-43. Transfer function estimation using the B-C aerial mode (0-300kHz)	180
Figure 5-44. Time domain signal and spectra recorded in the Sydney West scontrol room	181
Figure 5-45. Time domain signal and spectra recorded in the Bayswater substation control room	181
Figure 5-46. Comparison of step responses in the modal domain	182
Figure 6-1. Sectionalised view of a dead tank 'hair-pin' and a live head CT assembly [79, 80]	187
Figure 6-2. HV equivalent circuit of a high voltage current transformer	188
Figure 6-3. High frequency electrical model of a transformer winding [83]	190
Figure 6-4. High frequency model of a two-winding transformer	191
Figure 6-5. High frequency equivalent model referred to the high frequency side	191
Figure 6-6. High frequency model of a 'hair-pin' current transformer	192
Figure 6-7. Dismantled 330kV CT at Eraring	193
Figure 6-8. Nameplate from the dismantled current transformer	193
Figure 6-9. DC resistance measurement	194
Figure 6-10. Tests being conducted in the UTS laboratory	194
Figure 6-11. Depiction of the current density within close conductors, while carrying high frequency current in the same direction	196
Figure 6-12. Magnetising characteristic of the CT line protection core	197
Figure 6-13. Simulated A phase to earth fault at 40km on a 100km line	199

Figure 6-14. Capacitance of individual foil layers from a 330kV 'hair-pin' CT	200
Figure 6-15. Measurement of the stay capacitance using the step response approach	201
Figure 6-16. General arrangement of cabling within the bay marshalling kiosk	203
Figure 6-17. Cable cross sections (4 core 7/0.029" and 19 core 7/0.029" respectively)	203
Figure 6-18. Calculated resistance at various frequencies	206
Figure 6-19. Calculated inductance at various frequencies	206
Figure 6-20. Calculated capacitance at various frequencies	207
Figure 6-21. The application of a terminating short circuit	207
Figure 6-22. Driving point impedance of the secondary cabling	208
Figure 6-23. The application of a relay burden	209
Figure 6-24. Driving point impedance of the secondary cabling and the frequency independent relay burden	209
Figure 6-25. The Hathaway interposing current transformer	210
Figure 6-26. Magnetic flux generated within the interposing transformer	210
Figure 6-27. Experimental setup to determine the frequency response of the interposing CT	213
Figure 6-28. Frequency response of the interposing current transformer	213
Figure 6-29. The configuration of the Hathaway CT measurement scheme [21]	214
Figure 6-30. Experimental setup in the Sydney West 330kV substation control room	215
Figure 6-31. High frequency transient observed by the digital oscilloscope	215
Figure 6-32. High frequency transient observed by the travelling wave recorder	216
Figure 6-33. Simulated travelling wave transients for an A phase circuit breaker operation at Bayswater 330kV substation	217
Figure 6-34. Simulated circuit breaker transient signal for an A phase breaker pole operation.	218
Figure 6-35. Circuit breaker transient recorded by the travelling wave recorder for an A phase pole is operation at Bayswater.	219
Figure 7-1. Calculated pseudo-frequency at various scales for the sym2 wavelet with a sampling rate of 1.25MHz	223
Figure 7-2. Frequency response of current transformer, secondary cabling and relay burden compared to various CWT scales and DWT levels	224
Figure 7-3. DWT coefficients for a simulated incipient fault at 71.6km	225
Figure 7-4. DWT coefficients for an observed incipient fault at 71.6km	226
Figure 7-5. CWT coefficients for the simulated incipient fault at 71.6km	226
Figure 7-6. CWT coefficients for the observed incipient fault at 71.6km	227
Figure 7-7. Lattice diagram for a solid and incipient fault, respectively	228
Figure 7-8. Simulated CWT coefficients for an A phase to earth faults on a 100km circuit	229
Figure 7-9. Simulated solid A phase to earth fault at 56.7km on a 188.5km line	230
Figure 7-10. Simulated incipient lightning strike at 56.7km on a 188.5km line	231
Figure 7-11. CWT ² for a simulated solid fault at 56km	231
Figure 7-12. CWT ² for a simulated incipient fault at 56km	231
Figure 7-13. CWT ² Reflection distributions for simulated incipient and solid faults	232
Figure 7-14. CWT ² for a simulated solid fault at 56km	233
Figure 7-15. CWT ² for a simulated incipient fault at 56km	233
Figure 7-16. Observed solid fault at 49km on the Sydney West to Bayswater circuit	234
Figure 7-17. Observed incipient fault at 72km on the Sydney West to Bayswater circuit	234
Figure 7-18. CWT ² for an observed solid fault at 49km	235
Figure 7-19. CWT ² for an observed incipient fault at 72km	235
Figure 7-20. High impedance fault located 63.6km from the monitored busbar	236
Figure 7-21. Distribution in transient travelling times	237
Figure 7-22. CWT ² contour peaks for several observed incipient faults	239
Figure 7-23. CWT ² contour peaks for several observed solid faults	239
Figure 8-1. The Wellington 72 line reactor circuit breaker shortly after the failure in 1998	243
Figure 8-2. Bayswater power station	244
Figure 8-3. 132kV voltage and frequency observed at Sydney West following the initial fault	244
Figure 8-4. The Bayswater busbar configuration, and the associated switchyard	245
Figure 8-5. First fault and trip observed by the Regentville fault recorder (21:41:45)	245

Figure 8-6. Auto-reclose and trip observed by the Regentville fault recorder (21:41:59)	246
Figure 8-7. Second auto reclose observed by the Regentville fault recorder (21:42:01)	247
Figure 8-8. Phase fault observed by the Regentville fault recorder (21:43:44)	247
Figure 8-9. 220kV bushing with a 'caplink' installed, and the insulation from a failed 400kV bushing [110]	249
Figure 8-10. Radio based condition monitoring data recorded at Kemps Creek on the 9/6/1999	251
Figure 8-11. Results of a sensitivity test conducted at the TransGrid line training school	251
Figure 8-12. Capacitive transducer placed across the DLA test tap on a current transformer	253
Figure 8-13. DLA and leakage current measurements recorded on the 15 th November 2003	253
Figure 8-14. Leakage currents within the line 34 (Liddell) bus coupler CT	254
Figure 8-15. Leakage currents within the line 31 (Regentville) bus coupler CT	254
Figure 8-16. Leakage currents within the line 32 (Sydney West) bus coupler CT	255
Figure 8-17. General layout of the Bayswater switchyard showing the summated current transformer circuits used by the travelling wave recorder	256
Figure 8-18. The initial CT failure resulting in an A phase to earth fault	257
Figure 8-19. The reclose operation of the line breaker poles, and the resulting A phase to earth fault	257
Figure 8-20. The reclose operation of the coupler circuit breaker poles, and the A phase to earth fault	258
Figure 8-21. The resulting B to C phase fault	258
Figure 8-22. High frequency signals recorded prior to the failure	259
Figure 8-23. Signal spectra observed at Bayswater during the CT failure and for a prior fault	260
Figure 8-24. Test circuit for measurement across the tap of a bushing [113]	262
Figure 8-25. Example PD voltage signal for a narrow-band measuring device with a bandwidth of 10kHz and a mid-band frequency of 75kHz [113].	263
Figure 8-26. Proposed application of time thresholds T_1 and T_2	264
Figure 8-27. Typical pulse train observed during disconnect switch operation [120]	265
Figure 8-28. The TiePie Handyscope HS3 and the experimental setup	266
Figure 8-29. Observed noise using a 1MHz sampling rate and a 13.1ms window	267
Figure 8-30. Observed noise using a 5MHz sampling rate and a 2.6ms window	267
Figure 8-31. A short-duration transient observed on the CT secondary circuit	268
Figure 8-32. A longer duration transient observed on the CT secondary circuit	268
Figure 8-33. Prototype of the on-line monitor	269
Figure 8-34. Simulated frequency response of the filter using a 100mV variable frequency source	270
Figure 8-35. The schematic of the detection circuit	271
Figure 8-36. Circuit to simulate the discharge transient observed at Bayswater	273
Figure 8-37. PSPICE simulation of the test circuit	274
Figure 8-38. Observed signal created by the test circuit for an arbitrary signal magnitude and frequency	275
Figure 8-39. Signals measured at the input to the LM393 comparator	276
Figure 8-40. Output voltage from the LM393 comparator with a pulse repetition frequency of 1.7kHz	276
Figure 8-41. Connell Wagner's high voltage test laboratory	278
Figure 8-42. The 132kV current transformer obtained from Armidale 330kV switchyard	279
Figure 8-43. Connection to the CT secondary terminals	280
Figure 8-44. A dummy load equivalent of substation secondary cabling, calculated at 100kHz	281
Figure 8-45. The dummy load used in the experiment	281
Figure 8-46. A Dummy Load equivalent of substation secondary cabling, calculated at 100kHz	282
Figure 8-47. Amplified background noise recorded by the digital oscilloscope	283
Figure 8-48. The DLA test terminal, located on the main tank of the current transformer	284
Figure 8-49. Signals observed by the digital oscilloscope at a primary voltage of around 10kV	284
Figure 8-50. Incorporating a high voltage spark gap in the experimental setup	285
Figure 8-51. Escalation of discharges following the breakdown of insulation	286
Figure 8-52. Discharges observed over a 25ms window	287
Figure 8-53. Discharges observed at a slightly higher test voltage	287
Figure 8-54. Partial discharge measurements taken during the test	288
Figure 8-55. Partial discharge measurements taken during the test	288

Figure 9-1. An example overhead insulator string [126]	294
Figure 9-2. Propagation on high voltage transmission lines [126]	294
Figure 9-3. Voltages observed at the busbar	295
Figure 9-4. Charging currents observed at the busbar	295
Figure 9-5. A phase charging current observed at the busbar	296
Figure 9-6. Scale 1 Discrete wavelet transform using the 'Sym2' wavelet function	296
Figure 10-1. Phase to earth faults applied to the synchronised phasor algorithm	300
Figure 10-2. Phase to earth faults applied to the unsynchronised phasor algorithm	301
Figure 10-3. Phase to earth faults applied to the basic impedance algorithm	302
Figure 10-4. Phase to phase faults applied to the basic impedance algorithm	302
Figure 10-5. Phase to earth faults applied to the basic reactance algorithm	303
Figure 10-6. Phase to phase faults applied to the basic reactance algorithm	303
Figure 10-7. Phase to earth faults applied to the Takagi algorithm	304
Figure 10-8. Phase to phase faults applied to the Takagi algorithm	304

List of Tables

Table 2-1. Fault location methods	9
Table 2-2. Microprocessor based fault location methods	10
Table 2-3. Transposed and untransposed single circuit phase impedances	61
Table 2-4. Phasing and transposition of dual circuits	61
Table 3-1. Example soil resistivity for various soil conditions	88
Table 3-2. Algorithms considered in the statistical analysis	89
Table 3-3. Fault statistics [67]	95
Table 3-4. Assumed fault type probabilities	95
Table 3-5. Issues associated with algorithm selection	110
Table 3-6. Accuracy of several algorithms for faults on the Sydney West to Bayswater 330kV circuit where the fault location is known	111
Table 4-1. Impedances observed from Sydney South on lines 76 (Wallerawang) and 12 (Dapto)	117
Table 4-2. Positive sequence loop impedances for the Queensland to New South Wales Interconnector	132
Table 4-3. Observed impedance for a remote busbar fault with both lines in service	133
Table 4-4. Observed impedance for a remote busbar fault with one line out of service	133
Table 4-5. Observed impedance for a remote busbar fault with one line out of service and earthed for maintenance	133
Table 5-1. Techniques of trigger delay compensation	156
Table 5-2. Dominant pole locations	166
Table 6-1. DC Resistance of the CT windings	195
Table 6-2. Electrical parameters for the transformer model	202
Table 6-3. Electrical characteristics of the 4-core cabling	204
Table 6-4. Loads applied to the line protection core	208
Table 10-1. Source impedances used for the statistical comparison	305

Nomenclature

a	discrete wavelet scaling constant
a_0	continuous wavelet scaling constant
$a(t)$	weighting function (J. Marti distributed parameter modelling)
$A(\omega)$	propagation factor
$ACSR$	aluminium conductor, steel reinforced
ADC	analogue to digital converter
ATP	alternative transients program
b	wavelet transformation constant
C	capacitance, F
C_T	Clarke transformation matrix
C'	capacitance per unit length, Fm^{-1}
CT	current transformer
CVT	capacitive voltage transformer
CWT	continuous wavelet transform
DFT	discrete Fourier transform
DFR	digital fault recorder
DWT	discrete wavelet transform
DDF	dielectric dissipation factor
DLA	dielectric loss angle
ε_0	permittivity of free space, $8.85 \times 10^{-12} \text{ Fm}^{-1}$
ε_R	relative permittivity
e, \exp	base of natural logarithms
E	magnetising voltage, V
$EMTP$	electromagnetic transients program
EST	eastern standard time
FFT	fast Fourier transform
f	frequency
F	magneto-motive force
F_T	Fortescue transformation matrix
G	nodal conductance matrix
GE	General Electric Co.
GPS	global positioning system

h	height, m
HV	high voltage
I	current, A
$IEEE$	Institute of Electrical and Electronics Engineers
Im	operator; imaginary component of a complex parameter
j	$\sqrt{-1}$
k	an integer
K_T	Karenbauer transformation matrix
l	line length, m
L	inductance, H
L'	inductance per unit length, Hm^{-1}
l_C	span length, m
\ln	natural logarithm
m	fault location
n	an integer
M	mutual coupling
$MCBL$	minimum calculated breaking load
N	an integer, number of turns in a winding
P	per unit length potential matrix
PD	partial discharge
PVC	poly vinyl chloride
q_m	conductor charge
q	an integer
Q	charge, coulomb
r	radius, m
Re	operator; real component of a complex parameter
RCF	residual compensation factor
$SCADA$	system control and data acquisition
SC/GZ	steel conductor, zinc galvanised
SIR	source impedance ratio
SR	source ratio
$STFT$	short time Fourier transform
t, T	time, s
T	modal transformation matrix

T_C	conductor tension
ΔT	time step or relative change in time, s
T_S	sampling period, s
μ_0	permeability of free space, $4\pi \times 10^{-7} \text{ N.A}^{-2}$ (or $\text{Wb A}^{-1} \text{ m}^{-1}$, Hm^{-1})
μ_R	relative permeability
V	voltage, V
v	modal velocity
V_m	conductor potential
w_C	conductor weight per meter
w	window function
$\Delta\omega$	uncertainty in angular frequency
$WDFT$	windowed discrete Fourier transform
x	position, displacement
$x(t)$	a signal
Δx	incremental section of line
X	reactance, Ω
X/R	ratio of source reactance to resistance
XLPE	cross-linked polyethylene
Y	shunt admittance, siemens
Z	series impedance, Ω
Z_0	surge impedance, Ω

Greek

α	$1e^{j120}$
δ	synchronising angle
ϕ	flux linkage, Tm^{-2} (or webers)
γ	propagation constant, m^{-1}
λ	matrix of eigenvalues
π	pi
ρ	Earth resistivity, Ωm
τ	time delay, s
ω	radians per second
ψ	wavelet function

Subscripts

A	phase A (red phase)
B	phase B (white phase)
C	phase C (blue phase)
AA	self interaction on the A phase
BB	self interaction on the B phase
CC	self interaction on the C phase
AB	interaction between A and B phases
BC	interaction between B and C phases
CA	interaction between C and A phases
D	discharge
E	earth
E	excitation
E_A	cable sheath on the A phase
E_B	cable sheath on the B phase
E_C	cable sheath on the C phase
f	fault
L	line
M	mutual
R	remote busbar
S	series
X	phase X on a coupled circuit
Y	phase Y on a coupled circuit
Z	phase Z on a coupled circuit
$0, 00$	zero sequence
$1, 11$	positive sequence
$2, 22$	negative sequence

Symbols which are not defined above will be specified in the text.